Single-Crystal and Powder EPR Studies of the $S = {}^1/_2$ Ground State of the Iron−Sulfur Core in [Tris(tetraethylammonium)]-[tetrakis(benzylthiolato)tetrakis(μ_3-sulfido)tetrairon]·(*N*,*N*-Dimethylformamide) with Crystal Structure Determination

Jocelyne Gloux,[†] Pierre Gloux,*[,‡] and Jean Laugier

Contribution from the CEA/Département de Recherche Fondamentale sur la Matière Condensée, SCIB/SCPM, 38054 Grenoble Cedex 9, France

Received April 29, 1996[⊗]

Abstract: The crystal structure at room temperature of the solvated iron−sulfur synthetic compound $(Et_4N)_3[Fe_4S_4(SCH_2Ph)_4]$·DMF has been determined. The conformation of four ligand branches CH_2Ph linked to the Fe_4S_8 unit is very disturbed in contrast with the much more symmetrical situation in the already known nonsolvated compound. The paramagnetic core $[Fe_4S_4]^+$ has been studied by electron paramagnetic resonance (EPR) at a few kelvins in single crystals: it has an $S = {}^1/_2$ ground state in contrast with the $S = {}^3/_2$ ground state in the nonsolvated compound. It is the first $S = {}^1/_2$ ground state studied in a single crystal for an iron−sulfur synthetic compound and has g values of 2.027, 1.930, and 1.904 and principal directions near the three normals to opposite "faces" of the cubane $[Fe_4S_4]^+$. Polycrystalline EPR studies were done to observe alterations of the product but also are analyzed in relation with previous frozen solution studies.

Introduction

Analogs of the cores of the active site of iron−sulfur proteins have been synthesized in various laboratories in order to undertake the study of their physical properties. Polycrystalline solids or frozen solutions were prepared for magnetic susceptibility and magnetization measurements and for Mössbauer and EPR spectroscopy of the ground states. Holm and co-workers have synthesized and studied in particular reduced clusters $[Fe_4S_4(SR)_4]^{3-}$ and oxidized clusters $[Fe_4S_4(SR)_4]^{2-}$, which involve cores $[Fe_4S_4]^+$ and $[Fe_4S_4]^{2+}$ of cubane type respectively, like reduced and oxidized ferredoxins.[1]

The $[Fe_4S_4]^{2+}$ oxidation state (with even number of electrons) has a ground spin state $S = 0$. The $[Fe_4S_4]^+$ oxidation state (with odd number of electrons) has half-integer spins so EPR spectroscopy plays an important role in the study of the corresponding ground states. Our ambition is to improve knowledge of the spin ground states in such iron−sulfur synthetic compounds by proceeding to full EPR studies on single crystals in order to obtain the complete g-tensor in the molecular geometry and not just the g values as in the polycrystalline studies.

We have undertaken single-crystal EPR studies of the ground spin state in the two families of Fe_4S_4 clusters. First, by γ-irradiation of single crystals containing the diamagnetic $[Fe_4S_4]^{2+}$ oxidation state, we have created dilute $[Fe_4S_4]^+$ and $[Fe_4S_4]^{3+}$ oxidation states which up to now have always shown ground spin states $S = {}^1/_2$.[2] Second, we are developing EPR studies of single crystals containing the $[Fe_4S_4]^+$ oxidation state, which is more difficult but has the advantage of working on an intrinsic species whose geometry can be obtained by X-ray studies.

From polycrystalline solid studies in the $(R'_4N)_3[Fe_4S_4(SR)_4]$ compounds, Carney et al.[3] identify three categories of ground spin state behavior for the synthetic $[Fe_4S_4]^+$ oxidation state: (i) pure spins $S = {}^3/_2$ or $S = {}^1/_2$, (ii) physical mixtures of pure spins $S = {}^1/_2$ and $S = {}^3/_2$, (iii) spin-admixed states $S = "{}^1/_2 + {}^3/_2"$ of pure spins $S = {}^1/_2$ and $S = {}^3/_2$.

We have already reported a single-crystal EPR study of a synthetic $[Fe_4S_4]^+$ oxidation state involving an effective spin $S = {}^3/_2$ and its two Kramers doublets:[4] this was for the case of the ground spin state in the compound $(Et_4N)_3[Fe_4S_4(SCH_2Ph)_4]$, which Carney et al. class in their third category.[3] We found that the high concentration of the paramagnetic centers leads to spin−spin interactions that both enrich and complicate the EPR spectra as compared to those of the dilute paramagnetic species created by γ-irradiation in the diamagnetic crystals.

In the present paper, we report the new single-crystal EPR study of another synthetic $[Fe_4S_4]^+$ oxidation state, this time for the case of an effective spin $S = {}^1/_2$. We obtained the corresponding crystal as a variant after the synthesis of the compound $(Et_4N)_3[Fe_4S_4(SCH_2Ph)_4]$. The spin−spin interactions lead to more complex spectra than those of the first case. The present compound is much more unstable in air, which greatly increases the difficulty of obtaining results. Moreover, it was very difficult to make single crystals of sufficient quality for X-ray studies and for identification of the solvated compound $(Et_4N)_3[Fe_4S_4(SCH_2Ph)_4]$·DMF (where DMF designates a molecule of dimethylformamide $HCONMe_2$). But several attractive features motivate the study of this compound. Whereas the $S = {}^1/_2$ ground spin state alone is frequently encountered for the native $[Fe_4S_4]^+$ oxidation level in the reduced ferredoxins, this

* Author to whom correspondence should be addressed.
[†] Also at the University Joseph Fourier, Grenoble, France.
[‡] Also with CNRS, Grenoble, France.
[⊗] Abstract published in *Advance ACS Abstracts,* November 1, 1996.

(1) Berg, J. M.; Holm, R. H. In *Metal Ions in Biology*; Spiro, T. G., Ed.; Interscience: New York, 1982; Vol. 4, Chapter 1.
(2) (a) Gloux, J.; Gloux, P.; Lamotte, B.; Rius, G. *Phys. Rev. Lett.* **1985**, *54*, 599. (b) Gloux, J.; Gloux, P.; Hendriks, H.; Rius, G. *J. Am. Chem. Soc.* **1987**, *109*, 3220. (c) Gloux, J.; Gloux, P.; Lamotte, B.; Mouesca, J.-M.; Rius, G. *J. Am. Chem. Soc.* **1994**, *116*, 1953.
(3) (a) Carney, M. J.; Papaefthymiou, G. C.; Spartalian, K.; Frankel, R. B.; Holm, R. H. *J. Am. Chem. Soc.* **1988**, *110*, 6084. (b) Carney, M. J.; Papaefthymiou, G. C.; Frankel, R. B.; Holm, R. H. *Inorg. Chem.* **1989**, *28*, 1497.
(4) Gloux, J.; Gloux, P. *J. Am. Chem. Soc.* **1995**, *117*, 7513.

S0002-7863(96)01396-0 CCC: $12.00

Table 1. Crystal Data for $(Et_4N)_3[Fe_4S_4(SCH_2Ph)_4]\cdot DMF$

formula	$C_{55}H_{95}Fe_4S_8N_4O$
fw	1308.25
crystal system	orthorhombic
space group	$P2_12_12_1$
a (Å)	24.52 (1)
b (Å)	12.210 (5)
c (Å)	21.866 (6)
Z	4
R	0.080
GOF	1.28

is only the second time that such a state has been found alone in the synthetic compounds, and it is the first single-crystal EPR study. Also, it provides an occasion to characterize a new ground spin state following the earlier study of the state with effective spin $S = {}^3/_2$ for the same cluster $[Fe_4S_4(SCH_2Ph)_4]^{3-}$.

First, we will present the X-ray single-crystal structural study of the compound $(Et_4N)_3[Fe_4S_4(SCH_2Ph)_4]\cdot DMF$. After that, the powder and single-crystal EPR studies will constitute the main part of the paper.

Crystal Structure of $(Et_4N)_3[Fe_4S_4(SCH_2Ph)_4]\cdot DMF$

We obtained the corresponding crystals directly after the single-step synthesis method of Hagen et al.,[5] before the recrystallization in acetonitrile that leads to single crystals of the nonsolvated compound.

Solution and Description of the Structure. After introduction in a Lindemann capillary, which was sealed under argon, a crystal was studied at room temperature on an Enraf-Nonius CAD-4 diffractometer using graphite-monochromated Mo Kα radiation. After eliminating a number of samples of insufficient quality to get diffraction data, the X-ray study could be done on one crystal of approximate dimensions 0.7 × 0.35 × 0.3 mm. Although somewhat too big to be properly studied on the four-circle diffractometer, this sample was used just as it was. The cell parameters were refined by least-squares from the positions of 25 standard reflections. They are given in Table 1 with the other crystal data. The systematic absences that were recorded allowed us to identify the crystal space group as $P2_12_12_1$. In the intensity measurements, Lorentz and polarization corrections were taken into account, but no absorption correction was included. Using the direct method involved in the SHELX86 package,[6] all the atoms of $Fe_4S_4(SCH_2C_6H_5)_4$ were found except the hydrogen atoms. Difference Fourier maps then allowed us to locate all the non-hydrogen atoms of three $(C_2H_5)_4N$ units and of one solvate molecule $HCON(CH_3)_2$. Refinement was achieved with the program SHELX76.[7] Given the relatively low crystalline quality, only 3083 structure factors could be deduced from the 8555 measurements done. Also, we had to reduce the number of variables to be refined that would otherwise have reached the maximum of 649 for the full anisotropic model. On the one hand, the atoms of the cations and of the DMF molecule were refined for only isotropic thermal parameters. On the other hand, the atoms of the anion were refined for anisotropic thermal parameters, but with imposed rigid plane blocks for the phenyl cycles (C−C = 1.395 Å). The number of variables was thus reduced to 466. The hydrogen atoms were calculated but not refined. The final residual is $R_w = 0.07$.

(5) Hagen, K. S.; Watson, A. D.; Holm, R. H. *Inorg. Chem.* **1984**, *23*, 2984.

(6) Sheldrick, G. M. *Crystallographic Computing 3*; Sheldrick, G. M., Kruger, C., Goddard, R., Eds.; Oxford University Press: Oxford, U.K., 1985; p 175.

(7) Sheldrick, G. M. *SHELX76 System of Computing Programs*; University of Cambridge: Cambridge, England, 1976.

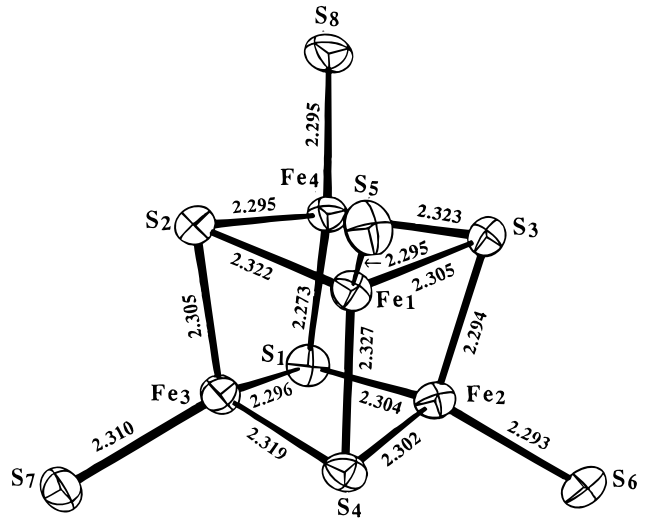

Figure 1. Structure of the Fe_4S_8 portion of the anion $[Fe_4S_4(SCH_2Ph)_4]^{3-}$ present in $(Et_4N)_3[Fe_4S_4(SCH_2Ph)_4]\cdot DMF$, showing the atom-labeling scheme and the iron−sulfur bond distances.

Knowledge of the X-ray structure was essential for two reasons: (1) to identify this compound with spin $S = {}^1/_2$ and to find the differences which characterize it in relation to the compound with spin $S = {}^3/_2$; (2) to have the geometry of the Fe_4S_4 cubane available so as to interpret the *g*-tensor measured by EPR.

The asymmetric unit consists of one anion $[Fe_4S_4(SCH_2Ph)_4]^{3-}$, three cations $(Et_4N)^+$, and one solvate molecule $HCONMe_2$. The differences between the compounds with spin $S = {}^1/_2$ and spin $S = {}^3/_2$ come from the capture of the solvate molecule in the compound with spin $S = {}^1/_2$. To give an idea of the distances between the Fe_4S_4 cubane and the nearest nitrogen-containing groups, we note that the shortest distances Fe−N and S−N for the nitrogens of the cations are about 5−5.3 and 4.5−5.5 Å, respectively, and that the nitrogen of the solvate molecule which is distinctly the nearest to the cubane is about 5.4 and 5 Å distant from an iron and a sulfur, respectively.

The atomic positions for the non-hydrogen atoms—the irons, sulfurs, and carbons of the anion; the nitrogen and carbons of the cations; the oxygen, nitrogen, and carbons of the solvate molecule—are reported in the Supporting Information. The structure of the Fe_4S_8 portion is shown in Figure 1 with the iron−sulfur bond distances, i.e., the four Fe−S and 12 Fe−S* distances (where S* is a core atom). More generally, Table 2 gives selected distances and angles of the Fe_4S_8 structure for the same categories as those given in ref 8 for the Fe_4S_8 structure of the nonsolvated compound. In the table, each category is divided into blocks, either one block of four or three blocks of two or three blocks of four. A possible D_{2d} symmetry would lead to the equivalence of the parameters in each block and, in the case of several blocks, to two groups involving respectively one block and two blocks, those of the same range for any parameter type. We clearly observe the equivalence (or the quasi-equivalence) of the means of the second and third blocks for all the parameter types of the $Fe_4S^*_4$ core. Thus, for an observation restricted to the mean values, the $Fe_4S^*_4$ cubane would exhibit a D_{2d} idealized symmetry. The three means of the Fe−S* distances (2.317, 2.300, and 2.300, respectively) would indicate that it is an elongated D_{2d} symmetry with the $\overrightarrow{Fe(1)Fe(2)} \times \overrightarrow{Fe(3)Fe(4)}$ direction as the $\bar{4}$ axis; we note also that the difference between the long and short values is so small that it would be one of the smallest differences known. But we find that the equivalence is not as good in the details of the

(8) Berg, J. M.; Hodgson, K. O.; Holm, R. H. *J. Am. Chem. Soc.* **1979**, *101*, 4586.

Table 2. Selected Distances (Å) and Angles (deg) for the Fe_4S_8 Portion of the Anion of $(Et_4N)_3[Fe_4S_4(SCH_2Ph)_4]\cdot DMF$[a]

Fe···S*		Fe−S	
Fe(1)−S(1)	3.900 (5)	Fe(1)−S(5)	2.295 (6)
Fe(2)−S(2)	3.930 (5)	Fe(2)−S(6)	2.293 (5)
Fe(3)−S(3)	3.919 (5)	Fe(3)−S(7)	2.310 (5)
Fe(4)−S(4)	3.917 (5)	Fe(4)−S(8)	2.295 (5)
mean	**3.917**	**mean**	**2.298**
Fe···Fe		**S*···S***	
Fe(1)−Fe(2)	2.777 (3)	S(1)−S(2)	3.593 (6)
Fe(3)−Fe(4)	2.757 (3)	S(3)−S(4)	3.613 (7)
mean	**2.767**	**mean**	**3.603**
Fe(1)−Fe(3)	2.750 (3)	S(1)−S(3)	3.636 (6)
Fe(2)−Fe(4)	2.745 (3)	S(2)−S(4)	3.685 (7)
mean	**2.748**	**mean**	**3.661**
Fe(1)−Fe(4)	2.730 (3)	S(1)−S(4)	3.659 (7)
Fe(2)−Fe(3)	2.745 (3)	S(2)−S(3)	3.685 (6)
mean	**2.738**	**mean**	**3.672**
mean of 6	2.751	mean of 6	3.645
Fe−S*		**S−Fe−S***	
Fe(1)−S(2)	2.322 (5)	S(5)−Fe(1)−S(2)	109.6 (2)
Fe(2)−S(1)	2.304 (5)	S(6)−Fe(2)−S(1)	114.9 (2)
Fe(3)−S(4)	2.319 (6)	S(7)−Fe(3)−S(4)	113.0 (2)
Fe(4)−S(3)	2.323 (5)	S(8)−Fe(4)−S(3)	109.6 (2)
mean	**2.317**	**mean**	**111.8**
Fe(1)−S(3)	2.305 (5)	S(5)−Fe(1)−S(3)	113.3 (2)
Fe(2)−S(4)	2.302 (5)	S(6)−Fe(2)−S(4)	118.2 (2)
Fe(3)−S(1)	2.296 (5)	S(7)−Fe(3)−S(1)	116.3 (2)
Fe(4)−S(2)	2.295 (4)	S(8)−Fe(4)−S(2)	113.2 (2)
mean	**2.300**	**mean**	**115.3**
Fe(1)−S(4)	2.327 (5)	S(5)−Fe(1)−S(4)	119.7 (2)
Fe(2)−S(3)	2.294 (5)	S(6)−Fe(2)−S(3)	108.9 (2)
Fe(3)−S(2)	2.305 (5)	S(7)−Fe(3)−S(2)	113.2 (2)
Fe(4)−S(1)	2.273 (5)	S(8)−Fe(4)−S(1)	118.7 (2)
mean	**2.300**	**mean**	**115.1**
mean of 12	2.305	mean of 12	114.1
Fe−S*−Fe		**S*−Fe−S***	
Fe(3)−S(1)−Fe(4)	74.2 (2)	S(3)−Fe(1)−S(4)	102.5 (2)
Fe(4)−S(2)−Fe(3)	73.7 (2)	S(4)−Fe(2)−S(3)	103.7 (2)
Fe(2)−S(3)−Fe(1)	74.3 (2)	S(2)−Fe(3)−S(1)	102.7 (2)
Fe(1)−S(4)−Fe(2)	73.7 (2)	S(1)−Fe(4)−S(2)	103.8 (2)
mean	**74.0**	**mean**	**103.2**
Fe(2)−S(1)−Fe(4)	73.7 (2)	S(2)−Fe(1)−S(4)	104.9 (2)
Fe(3)−S(2)−Fe(1)	72.9 (2)	S(3)−Fe(2)−S(1)	104.5 (2)
Fe(4)−S(3)−Fe(2)	73.0 (2)	S(4)−Fe(3)−S(2)	105.7 (2)
Fe(1)−S(4)−Fe(3)	72.6 (2)	S(1)−Fe(4)−S(3)	104.6 (2)
mean	**73.1**	**mean**	**104.9**
Fe(2)−S(1)−Fe(3)	73.3 (2)	S(2)−Fe(1)−S(3)	105.6 (2)
Fe(4)−S(2)−Fe(1)	72.5 (2)	S(4)−Fe(2)−S(1)	105.2 (2)
Fe(1)−S(3)−Fe(4)	72.3 (2)	S(1)−Fe(3)−S(4)	104.9 (2)
Fe(3)−S(4)−Fe(2)	72.9 (2)	S(3)−Fe(4)−S(2)	105.9 (2)
mean	**72.8**	**mean**	**105.4**
mean of 12	73.3	mean of 12	104.5
Fe−Fe−Fe		**S*−S*−S***	
Fe(3)−Fe(1)−Fe(4)	60.4 (1)	S(3)−S(1)−S(4)	59.4 (1)
Fe(4)−Fe(2)−Fe(3)	60.3 (1)	S(4)−S(2)−S(3)	58.7 (1)
Fe(2)−Fe(3)−Fe(1)	60.7 (1)	S(2)−S(3)−S(1)	58.8 (1)
Fe(1)−Fe(4)−Fe(2)	61.0 (1)	S(1)−S(4)−S(2)	58.6 (1)
mean	**60.6**	**mean**	**58.9**
Fe(2)−Fe(1)−Fe(4)	59.8 (1)	S(2)−S(1)−S(4)	61.1 (1)
Fe(3)−Fe(2)−Fe(1)	59.7 (1)	S(3)−S(2)−S(1)	59.9 (1)
Fe(4)−Fe(3)−Fe(2)	59.8 (1)	S(4)−S(3)−S(2)	60.6 (1)
Fe(1)−Fe(4)−Fe(3)	60.1 (1)	S(1)−S(4)−S(3)	60.0 (1)
mean	**59.9**	**mean**	**60.4**
Fe(2)−Fe(1)−Fe(3)	59.6 (1)	S(2)−S(1)−S(3)	61.3 (1)
Fe(4)−Fe(2)−Fe(1)	59.3 (1)	S(4)−S(2)−S(1)	60.3 (1)
Fe(1)−Fe(3)−Fe(4)	59.4 (1)	S(1)−S(3)−S(4)	60.6 (1)
Fe(3)−Fe(4)−Fe(2)	59.9 (1)	S(3)−S(4)−S(2)	60.6 (1)
mean	**59.6**	**mean**	**60.7**
mean of 12	60.0	mean of 12	60.0

[a] Their estimated standard deviations are in parentheses.

Table 3. Ranges of Values of Selected Distances (Å) and Angles (deg) of the Same Type in the Two Fe_4S_8 Portions of the Anions of the Solvated and Nonsolvated $(Et_4N)_3[Fe_4S_4(SCH_2Ph)_4]$

	range of values	
distances (Å)	solvated compd	nonsolvated compd[a]
Fe−S*	2.27−2.33	2.30−2.33
Fe−S	2.29−2.31	2.28−2.31
Fe···Fe	2.73−2.78	2.72−2.78
S*···S*	3.59−3.69	3.63−3.71
Fe···S*	3.90−3.93	3.91−3.96
	range of values	
angles (deg)	solvated compd	nonsolvated compd[a]
S−Fe−S*	108.9−119.7	107.4−119.8
S*−Fe−S*	102.5−105.9	103.2−106.5
Fe−S*−Fe	72.3−74.3	71.8−74.3
Fe−Fe−Fe	59.3−61.0	58.7−60.9
S*−S*−S*	58.6−61.3	59.1−61.2

[a] Deduced from data of ref 8.

parameters: there are notable exceptions as, for instance, in the group having mean value 2.300 for the Fe−S* distances, 2.327 for Fe(1)−S(4), and 2.273 for Fe(4)−S(1). Seeing only the mean values of the S−Fe−S* angles (respectively 111.8, 115.3, and 115.1°), we might have extended the D_{2d} idealized symmetry to the whole $S_4Fe_4S^*_4$ cluster, but in fact the parameters taken in detail do not obey this symmetry, and finally it is only possible, in each block, to group them two by two, on the one hand the first and fourth parameters, on the other hand the second and third. Then, if we include the outer S atoms, we can no longer retain D_{2d} symmetry with the $\bar{4}$ axis in the $\overrightarrow{Fe(1)Fe(2)} \times \overrightarrow{Fe(3)Fe(4)}$ direction but only an idealized 2-fold axis in the $\overrightarrow{Fe(1)Fe(4)} \times \overrightarrow{Fe(2)Fe(3)}$ direction.

Comparison between Solvated and Nonsolvated Structures. The various ranges of values of selected distances and angles of the same category for the Fe_4S_8 portions of the solvated (this work) and nonsolvated (ref 8) compounds are reported in Table 3, and we observe as a general rule a close analogy between the two series of values. To go further, we try to find a situation of superposition between the $Fe_4S^*_4$ "solvated" and "nonsolvated" cubanes that involves congruences between the two series of parameters. That would allow us to characterize the common configuration if it exists. A first group of 12 configurations of the $Fe_4S^*_4$ solvated cubanes is constituted by the atom labeling chosen in such a way that $\overrightarrow{Fe(1)Fe(2)}$, $\overrightarrow{Fe(1)Fe(3)}$, $\overrightarrow{Fe(1)Fe(4)}$ is a right-handed system in the structure and the labelings resulting from the 11 permutations of the atom labels that maintain the above system right-handed. We compare the parameters of each configuration with those of the same name of the particular nonsolvated cubane given in ref 8, which also has a right-handed system $\overrightarrow{Fe(1)Fe(2)}$, $\overrightarrow{Fe(1)Fe(3)}$, $\overrightarrow{Fe(1)Fe(4)}$. A second group of configurations is constituted by the labelings resulting from the 12 permutations of the atom labels that change the handedness of the system $\overrightarrow{Fe(1)Fe(2)}$, $\overrightarrow{Fe(1)Fe(3)}$, $\overrightarrow{Fe(1)Fe(4)}$. We then compare their parameters with those of the other type of nonsolvated cubanes, which has a left-handed system $\overrightarrow{Fe(1)Fe(2)}$, $\overrightarrow{Fe(1)Fe(3)}$, $\overrightarrow{Fe(1)Fe(4)}$. No association leading to a real correlation between the $Fe_4S^*_4$ solvated and nonsolvated cubanes comes out clearly from these comparisons between parameters. It is only when we extend the procedure to the outer S atoms, that is when we consider the $S_4Fe_4S^*_4$ clusters, that a more marked correlation appears in the case of a configuration of the first group. This is the one that is obtained by replacing the labeling (1,2,3,4) by the labeling (1,4,2,3): we find in this case close values for angles S−Fe−S* of the same label with a mean deviation of 1.3°. In this particular configuration of the $Fe_4S^*_4$ solvated

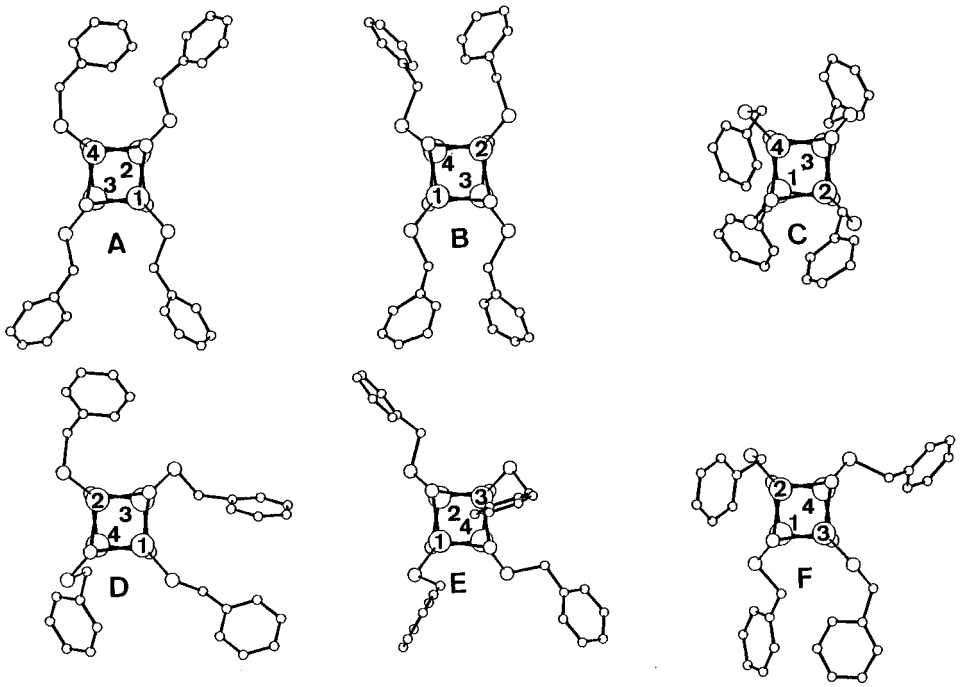

Figure 2. Views of the anion $[Fe_4S_4(SCH_2Ph)_4]^{3-}$ projected along the normals to opposite faces of the cubane, which form a quasi-orthogonal axis set. Case of the nonsolvated compound $(Et_4N)_3[Fe_4S_4(SCH_2Ph)_4]$ (from data of ref 8): (A) along $\overrightarrow{-Fe(1)Fe(4)} \times \overrightarrow{Fe(2)Fe(3)}$; (B) along $\overrightarrow{Fe(1)Fe(2)} \times \overrightarrow{Fe(4)Fe(3)}$; (C) along $\overrightarrow{Fe(1)Fe(3)} \times \overrightarrow{Fe(4)Fe(2)}$. Case of the solvated compound $(Et_4N)_3[Fe_4S_4(SCH_2Ph)_4]\cdot$DMF (this work): (D) along $\overrightarrow{-Fe(1)Fe(2)} \times \overrightarrow{Fe(3)Fe(4)}$; (E) along $\overrightarrow{Fe(1)Fe(3)} \times \overrightarrow{Fe(2)Fe(4)}$; (F) along $\overrightarrow{Fe(1)Fe(4)} \times \overrightarrow{Fe(2)Fe(3)}$. The labeling (1,2,3,4) of the irons of a solvated cubane is in correspondence with the labeling (1,4,2,3) of the irons of the nonsolvated cubane placed above it in the figure, following the connection that is discussed in text.

cubane, the idealized 2-fold axis in the $\overrightarrow{Fe(1)Fe(4)} \times \overrightarrow{Fe(2)Fe(3)}$ direction considered above comes parallel to the idealized 2-fold axis in the $\overrightarrow{Fe(1)Fe(3)} \times \overrightarrow{Fe(2)Fe(4)}$ direction introduced in ref 8 for the nonsolvated cubane.

The addition of the solvate molecule induces serious structural changes in the environment of the cubane. First, there is the presence of the solvate molecule itself at about 5 Å from the cubane. There are the very different space groups, monoclinic *Cc* for the nonsolvated case and orthorhombic $P2_12_12_1$ for the solvated case, producing very different environments of anionic neighbor sites around each anion considered. There are also the very different orientations, with respect to each central cubane, of the terminal ligands of the anions beyond the four outer sulfurs together with the different locations found for the nearest cations. In the analysis of the orientation of the terminal ligands, it is usual to introduce the dihedral angles S*−Fe−S−C and to examine whether they approach the 180° staggered position where the S−C bond is opposite to a Fe−S* bond; the other limiting case would correspond to the position where the S−C bond eclipses a Fe−S* bond.[9] In the nonsolvated case, the conformation of the terminal ligands obeys a certain ordering, which consists of approaching the 180° staggered position for the four angles situated in the range 162−180° and with regard to the four Fe−S* bonds "parallel" to the normal to opposite faces of the cubane $\overrightarrow{Fe(1)Fe(3)} \times \overrightarrow{Fe(2)Fe(4)}$. Then, the four ligands are deployed "parallel" to this direction as we see in Figure 2, where we show views of the anion projected along the three normals to opposite faces of the cubane, which form a quasi-orthogonal axis set. In addition, it appears that the nearest cations, which are four in number, lie above the four other cubane faces with distances Fe−N grouped around 5 Å and distances S−N about 4.5−5 Å. On the other hand, here in this solvated compound, the conformation of the terminal ligands appears strongly disordered. Two terminal ligands approach the staggered position with regard to Fe−S* directions that appear a priori arbitrary, with dihedral angles of 170° for S*(3)−Fe(4)−S(8)−C(8) and 174° for S*(3)−Fe(2)−S(6)−C(6). The two other terminal ligands approach the eclipsed position with dihedral angles of 22° for S*(2)−Fe(1)−S(5)−C(5) and only 4° for S*(2)−Fe(3)−S(7)−C(7)! In Figure 2 where, as for the nonsolvated case, we show views of the anion projected along the normals, we can only note the considerable changes from one case to the other. The location of the cations is also seriously affected: the nearest cations no longer lie two by two above opposite faces, but instead the three nearest cations are connected to three orthogonal faces and less well aligned with these faces. Among the 10 sulfurated or seleniated compounds whose structure is now known, this is certainly the one that presents the biggest disorganization with regard to the orientation of terminal ligands of the anion $[Fe_4X_4(SR)_4]^{3-}$ (X = S, Se), whereas the nonsolvated compound is among those that involve the best structured anions. Most of the eight other known structures involve $[Fe_4X_4(SR)_4]^{3-}$ anions with terminal ligands for which the four dihedral angles X*−Fe−S−C approach the 180° staggered position. But, only in two or three of these structures are the four relevant Fe−X* bonds "parallel" to a same $\overrightarrow{Fe(i)Fe(j)} \times \overrightarrow{Fe(k)Fe(l)}$ direction as they are in the nonsolvated compound. Among the two or three structures where some dihedral angles deviate more from the staggered position, we note that up to now the dihedral angle that led to the situation nearest to an eclipsed position was 18° in the compound $(Et_3MeN)_3[Fe_4S_4(SPh)_4]$.[10] Only two other dihedral angles led to situations somewhat nearer an eclipsed position than a staggered position with the common value of

(9) In ferrous rubredoxin and the model complex $(Et_4N)_2[Fe(SR)_4]$ (R = 2-(Ph)C_6H_4), the splitting of the ferrous 3d orbitals is found to depend on the orientation of the S−C bond (Gebhard, M. S.; Koch, S. A.; Millar, M.; Devlin, F. J.; Stephens, P. J.; Solomon, E. I. *J. Am. Chem. Soc.* **1991**, *113*, 1640).

(10) Laskowski, E. J.; Frankel, R. B.; Gillum, W. O.; Papaefthymiou, G. C.; Renaud, J.; Ibers, J. A.; Holm, R. H. *J. Am. Chem. Soc.* **1978**, *100*, 5322.

28° in the compound $(Et_4N)_3[Fe_4S_4(S\text{-}p\text{-}C_6H_4Br)_4]$,[11] the first compound found with a spin $S = {}^1/_2$.

EPR Spectroscopy

Preserving the samples was a serious constraint, and precautions had to be increased as compared to work on the more stable nonsolvated compound. We have already seen that it had been hard to find a single crystal of acceptable quality for the X-ray study. Fortunately, the requirements were not as demanding for EPR studies, and the sample quality generally remained satisfactory if we took care to avoid keeping the samples too long in the glovebox and limited handling in air to a minimum during the EPR experiments.

EPR absorption measurements were done on a Varian E-109 X-band spectrometer equipped with an Oxford Instruments ESR-9 continuous-flow helium cryostat. The high concentration of electron spins produced spin−spin interactions, which induced broad lines and line splittings as in the case of the nonsolvated $S = {}^3/_2$ compound. However, as expected for a lower spin where spin−spin interactions are a priori weaker, the lines were less strongly broadened, less than 10 mT here compared to 10−30 mT in the $S = {}^3/_2$ case. Also, spin−lattice relaxation was much less troublesome than in the $S = {}^3/_2$ case, which leads us to think that the first excited states do not lie as low here. Whereas in the $S = {}^3/_2$ case the EPR lines were already broadened by spin−lattice relaxation at less than 10 K and disappeared above 12 K, here the lines are still seen to 30 K, even if broadened. Nevertheless, the experiments were done at very low temperature, generally near 4 K. As usual for powder samples, first-derivative spectra were recorded. For the single-crystal samples, second-derivative spectra obtained from "in phase" detection at the second harmonic of the Zeeman modulation frequency were preferred to facilitate measuring the resonance peaks to obtain the variations of the resonance fields as a function of orientation. The reduction of the amplitude of the EPR lines in the second-derivative mode could be compensated by increasing the microwave power.

Powder EPR Experiments. Figure 3A shows the powder EPR first-derivative absorption spectrum. The only signal present appears in a limited range around $g = 2$, which identifies unquestionably a spin $S = {}^1/_2$. The baseline retraced with gain × 100 for g above 3.5 gives no trace of any component of signals of other half-integer spins $S > {}^1/_2$.[12] The powder spectrum appears to correspond to axial symmetry, but we shall see that its appearance is misleading: the later single-crystal EPR results lead to a rhombic g-tensor with three distinct g values that are marked in Figure 3A. An extra signal attributed to a free radical impurity is observed at $g = 2$ as is often the case in model compounds with cluster trianion salts (see footnote 27 in ref 13).

It is interesting to examine in the powder EPR spectra two types of alteration of the material. First, Figure 3B shows the EPR spectrum of a polycrystalline sample that has remained in the glovebox a sufficiently long time to cause an alteration: signals appear at $g = 4.97$ and $g = 1.41$, i.e., at two of the three powder g values of the nonsolvated $S = {}^3/_2$ compound, and the third g value (1.9) would then be hidden by the $S = {}^1/_2$ signal.[14] We can deduce that the compound is unstable and that desolvation has operated on a fraction of the powder.

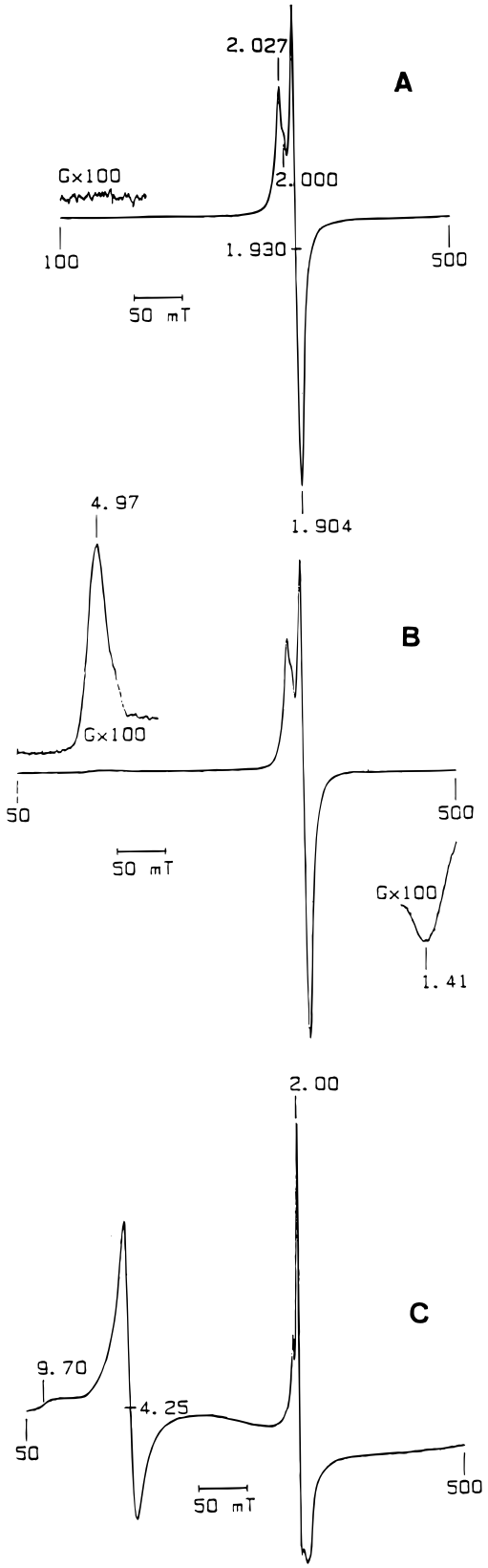

Figure 3. First derivative of the powder X-band EPR absorption for $(Et_4N)_3[Fe_4S_4(SCH_2Ph)_4]\cdot DMF$; frequency 9.23 GHz; modulation amplitude 1 mT; power 0.02 mW (A and B), 1 mW (C). (A) Typical spectrum: the 3 g values of the spin $S = {}^1/_2$ deduced from single-crystal EPR studies are marked; extra, free radical signal is observed at $g = 2$; the baseline with gain × 100 above $g = 3.5$ gives no trace of spins $S > {}^1/_2$. (B) Excessive time in the glovebox: gain × 100 shows features at $g = 4.97$ and 1.41 characteristic of the spin $S = {}^3/_2$ of nonsolvated $(Et_4N)_3[Fe_4S_4(SCH_2Ph)_4]$. (C) Excessive time in air: features at $g = 4.25$ and $g = 9.70$ are characteristic of a pure spin $S = {}^5/_2$ of Fe^{3+} ion where the rhombicity parameter is very close to the maximum; the extra signal at $g = 2$ is now considerably amplified.

(11) Stephan, D. W.; Papaefthymiou, G. C.; Frankel, R. B.; Holm, R. H. *Inorg. Chem.* **1983**, *22*, 1550.

(12) The magnetic susceptibility follows an $S = {}^1/_2$ Curie−Weiss law at low temperature, so excited states are not thermally accessible and thus are not observed by EPR.

(13) Laskowski, E. J.; Reynolds, J. G.; Frankel, R. B.; Foner, S.; Papaefthymiou, G. C.; Holm, R. H. *J. Am. Chem. Soc.* **1979**, *101*, 6562.

Second, Figure 3C shows the EPR spectrum of another polycrystalline sample that has remained overnight in air: there are severe modifications in the range around $g = 2$ with a large amplification of the free radical impurity signal, and moreover a strong signal of first-derivative shape is now observed at $g = 4.25$. This new signal has to be attributed to a (quasi-)isotropic effective g-tensor, and we can identify it with the effective g-tensor of the Kramers doublet "$\pm^3/_2$" of a pure spin $S = {}^5/_2$ when nonaxiality is very close to its maximum extent (isotropic $g = 4.29$).[15] The weak singularity around $g = 9.7$, which is situated at the edge of a broad signal, corresponds to the g value of 9.68 that is found for the two other Kramers doublets "$\pm^1/_2$" and "$\pm^5/_2$" of the $S = {}^5/_2$ spin when the nonaxiality is maximum; the weakness of the singularity expresses the small value of the transition probability given the smallness of the two other g values (0.86 and 0.61).[15] Moreover, this $S = {}^5/_2$ spectrum has a close analogy with the spectrum of Fe^{3+} ions in glass shown by Castner et al. in Figure 1 of ref 16. Thus, a large fraction of the compound is altered such that exchange and double-exchange interactions, which are assumed to operate on the high spins $S = {}^5/_2$ of the two Fe^{3+} and $S = 2$ of the two Fe^{2+} to give the $S = {}^1/_2$ spin, are not effective, and this leads to observation of only the high spins $S = {}^5/_2$ of the Fe^{3+} ions.

Single-Crystal EPR Experiments. In the single-crystal EPR studies, handling of the sample in air had to be reduced to a minimum given its fragility and its oxygen sensitivity. Also, the most developed face of the sample, parallel to the plane *bc* and with one edge parallel to the **b** axis, was fixed by grease on a small plate of plexiglass with the **b** axis edge oriented parallel to one edge of the plate by positioning against a shoulder. Then, on the bottom of a cylindrical sample-holder having two horizontal and vertical cuts, the plate could be fixed successively in three distinct orientations to get the angular variations of the resonance fields in the three mutually orthogonal planes *ab*, *bc*, and *ca*. Sample-holders with skew cuts allowed study in more general planes. Several single crystals were used during these experiments and gave consistent results.

The angular variations of the resonance fields in the three planes *ab*, *bc*, and *ca* are given in Figure 4, in millitesla. The EPR sites are all equivalent for **H** along the 2-fold axes, that is the **a**, **b**, and **c** crystal directions, and we note that the peak−peak widths of the first-derivative signal in these directions are about 30, 55, and 17 G, respectively. Because of the orthorhombic Laue symmetry, which leads to four distinguishable EPR sites when **H** is in a general direction, only two distinct EPR sites, i.e., two distinct angular variations, must appear in the *ab*, *bc*, and *ca* planes. This is indeed what is observed in the *ca* plane, and Figure 6A gives a typical spectrum showing the two corresponding lines in the absorption second-derivative mode. This spectrum corresponds to **H** in the *ca* plane at 38.5° to **c**. The same occurs in the *bc* plane even if the two angular variations fortuitously coalesce, which implies that the nondiagonal element $(g^2)_{bc}$ of the squared tensor $\mathbf{g^2}$ is zero. The behavior is more complicated in the *ab* plane: near the axes **a** and **b** one finds only one angular variation, just as in the *bc* plane, but over several tens of degrees, in the central part of the spectrum, four lines appear that are indicated by four series of dots in Figure 4. Spin−spin interactions between neighboring cubanes must be responsible for this splitting as was already

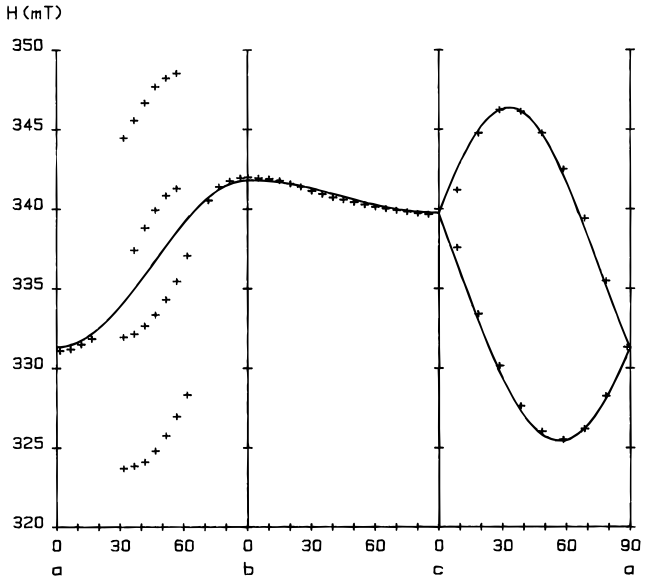

Figure 4. Experimental values (crosses) and fitted angular variations (curves) of the resonance fields in millitesla in the three orthogonal planes *ab*, *bc*, and *ca*. Microwave frequency is 9.23 GHz. The splittings by spin−spin interactions observed in the plane *ab* are not considered in the fit. The low-field curve in the plane *ca* corresponds to the EPR site of Table 4.

the case for other splittings between neighboring cubanes in the $S = {}^3/_2$ nonsolvated compound. The shortest center-to-center distances are of the same order, a little longer here (about 12.2−12.4 Å) than in the nonsolvated compound (about 11.3−11.5 Å), with the shortest iron−iron distances of 10.1 and 9.6 Å, respectively. The interactions mask information useful in the g-tensor calculation because we do not really know if in their absence the *ab* plane angular variation would be unique as the single variation observed near the **a** and **b** axes suggests. If it was unique, the nondiagonal element $(g^2)_{ab}$ would be zero, like $(g^2)_{bc}$, and the g-tensor would have the **b** axis as a principal axis, with at the most only two distinct EPR sites for **H** parallel to a general direction and thus only two lines in the absence of the spin−spin interaction splittings.

We have examined the angular variations in other more general planes. Figure 5, panels A and B, shows angular variations obtained with the plate of plexiglass fixed on a skew sample-holder section making an angle of about 30° with the horizontal plane, and the plate is rotated 90° on the section between the two experiments. The sample is fixed by grease on the shoulder of the plate of plexiglass: the **b** axis edge remains in its orientation parallel to the plate, but the *bc* plane face becomes perpendicular to the plate. The plane of Figure 5A is identified later as $a'b'$ with $\mathbf{a}'$ very close to **a** and $\mathbf{b}'$ at 32.5° to **b** in the plane *bc*. The plane of Figure 5B is a plane ba'' with $\mathbf{a}''$ at 59.5° to **c** in the plane *ca*. In the two cases, splittings by spin−spin interactions intervene to complicate the experimental angular variations, and moreover partial overlaps of too broad lines distort these variations. Figure 6B presents the spectrum for **H** parallel to the direction common to the two planes $a'b'$ and ba'', i.e., the direction oriented at 134° to $\mathbf{a}'$ in the plane $a'b'$ and at 53° to **b** in the plane ba''. In this direction, we observe essentially two lines of equal amplitude and a third line with about twice their amplitude, the three lines having equivalent widths. The strength of the latter, more intense line is preserved in both planes $a'b'$ and ba'', and this unique angular variation has to be associated with two equivalent EPR sites. Thus, the two EPR sites already equivalent by symmetry for **H** in the plane *ca* also appear equivalent for **H** in the plane ba'' and in all of the large part of the plane $a'b'$ where the splittings by spin−spin interactions are absent. These properties alone

(14) This set of values cannot be fitted by the diagrams of effective g values in terms of the rhombicity λ given in ref 15 for the Kramers doublets of a pure spin $S = {}^3/_2$ (isotropic real g value of 2). We explained the g value set by an effective spin $S = {}^3/_2$ with $\lambda \cong {}^1/_3$ and real g values around 1.9 (see ref 4).

(15) Hagen, W. R. In *Advances in Inorganic Chemistry*; Sykes, A. G., Ed.; Academic Press: New York, 1992; Vol. 38, p 165.

(16) Castner, T., Jr.; Newell, G. S.; Holton, W. C.; Slichter, C. P. *J. Chem. Phys.* **1960**, *32*, 668.

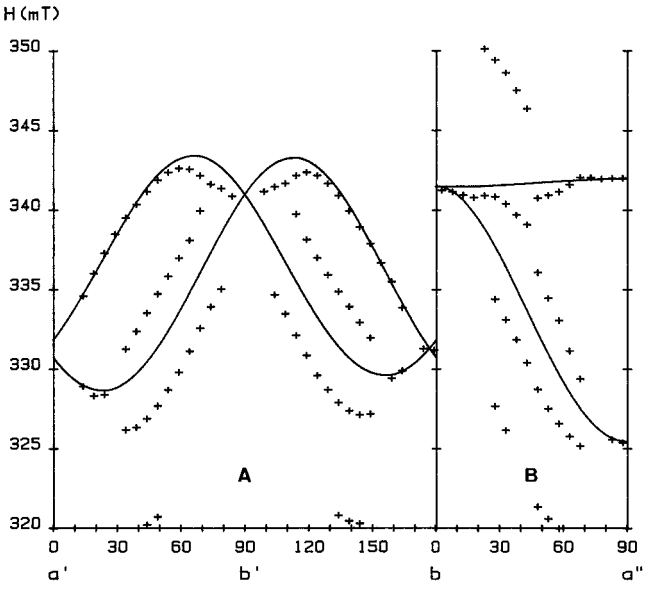

Figure 5. Experimental values (crosses) and fitted angular variations (curves) of the resonance fields in millitesla in planes *a′b′* and *ba″*. Microwave frequency is 9.23 GHz. The splittings by spin−spin interactions are not considered in the fit. (A) **H** in the plane *a′b′* whose normal has direction cosines (−0.035; −0.537; 0.843) in the axis system **abc**, with **a′** close to **a** and **b′** at 32.5° to **b** in the plane *bc*; the curve that lies in high field between 0° and 90° corresponds to the EPR site of Table 4. (B) **H** in the plane *ba″* whose normal has direction cosines (0.508; 0; −0.862) in the axis system **abc**, with **a″** at 59.5° to **c** in the plane *ca*; the low-field curve corresponds to the EPR site of Table 4.

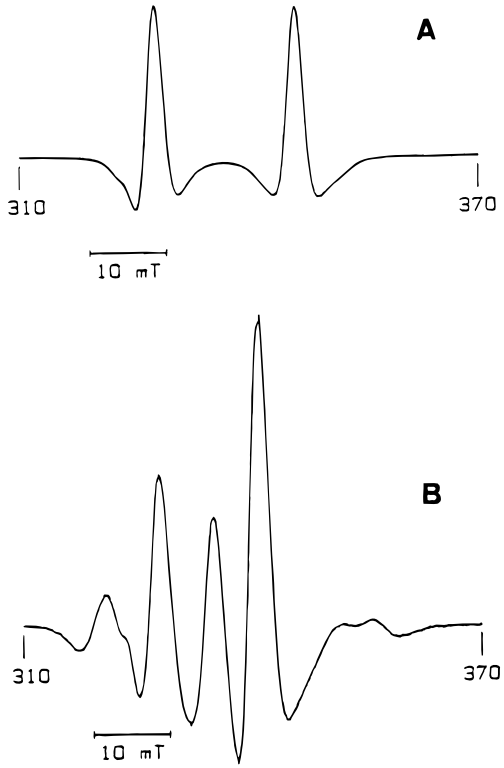

Figure 6. Second derivative of the EPR absorption. Modulation amplitude is 1 mT, and microwave power is 10 mW. (A) **H** parallel to the direction having orientation 38.5° to **c** in the plane *ca* of Figure 4; the lines of two EPR sites are clearly observed and show no splittings by spin−spin interactions. (B) **H** parallel to the direction common to the two planes *a′b′* and *ba″* of Figure 5, which is the direction oriented at 134° to **a′** in the plane *a′b′* and at 53° to **b** in the plane *ba″*; the lines of two EPR sites are observed, but the low-field line is split by spin−spin interaction.

are already sufficient to conclude that the EPR sites are equivalent two by two for **H** along any direction and the *g*-tensor has quite accurately the **b** axis as principal axis with zero nondiagonal elements $(g^2)_{ab}$ and $(g^2)_{bc}$. We note that the two lines of equal intensity and the corresponding angular variations in the plane *a′b′* could only be explained by a spin−spin interaction splitting because they were prolonged in another portion of the plane by the single line of equivalent sites, whereas an ordinary splitting of nonequivalent sites would have also been conceivable a priori if only the angular variations in the plane *ba″* were available.

The *g*-Tensor. The spin Hamiltonian in the case of a spin $S = {}^1/_2$ is simply the Zeeman Hamiltonian

$$H = \beta \mathbf{HgS} \qquad (1)$$

where β is the Bohr magneton. Using the analytic expression of the resonance field, which derives from eq 1 and which involves the matrix elements of the squared tensor $\mathbf{g^2}$ in the system of axes **abc** as parameters, least-square fits of angular variations are performed to obtain these parameters. The proceedings are facilitated in this case because we know that the elements $(g^2)_{ab}$ and $(g^2)_{bc}$ are zero. We note a particular point: in any direction showing spin−spin interaction splitting and considering the weakness of this spin−spin coupling as compared to the Zeeman coupling, the field value introduced in the calculation was taken as the average of the resonance fields. In the final fit, we used the angular variations in the three planes *ab*, *bc*, and *ca* of Figure 4 as well as the variations in the plane *ba″* of Figure 5B with **a″** at 59.5° from **c** in the plane *ca* and the variations in another plane involving **b**, i.e., the plane *bc′* with **c′** at 20° from **c** in the plane *ca*. Using the resultant matrix elements of the tensor $\mathbf{g^2}$, least-square fits of the angular variations in the plane *a′b′* of Figure 5A, now with the orientation parameters as the fitting parameters, allowed us to identify this plane as the one whose normal has direction cosines (−0.035; −0.537; 0.843) in the system of axes **abc** (with **a′** very close to **a** and **b′** at 32.5° from **b** in the plane *bc*). In Figures 4 and 5, fitted angular variations can be compared to the experimental points or to the mean positions between the points in the case of spin−spin interaction splitting.

From diagonalization of the $\mathbf{g^2}$ matrix, principal values and principal directions of the tensor **g** of one of two distinct EPR sites were obtained in the system of axes **abc** and are given in Table 4. To get the other EPR site, we exchange the sign of the direction cosines of absolute value 0.546. Single-crystal *g* values (2.027, 1.930, 1.904) prove the rhombicity of the *g*-tensor whereas the poor resolution of the powder EPR spectrum would have led us to deduce only an axial *g*-tensor. The *g* value 1.904 is too close to the value 1.930 for the usual signal observed for the minimum *g* value to appear in the powder spectrum.

Analysis of Results

***g* Value Comparisons with Other Intrinsic $[Fe_4S_4]^+$ of Spin $S = {}^1/_2$.** As a general rule, the spins $S = {}^1/_2$ found for $[Fe_4S_4]^+$ cubanes in the iron−sulfur proteins in frozen solutions belong to the "$g = 1.94$" type,[15] that is, systems having the intermediate *g* value around 1.93−1.94, while g_{av}, the average *g*, is somewhat bigger, around 1.96−1.97. The higher *g* value is around 2.04−2.07, and the lower *g* value is around 1.88−1.91. Thus, the spin under consideration with *g* values 2.027, 1.930, and 1.904 and $g_{av} = 1.954$ conforms well to the type, even if the higher *g* value is at the lower limit. In $(Et_4N)_3[Fe_4S_4(S\text{-}p\text{-}C_6H_4Br)_4]$, the other synthetic compound where a spin $S = {}^1/_2$ is found alone, the powder *g* values are 2.05, 1.93, and 1.89 and $g_{av} = 1.96$.[11]

Generally, a spin $S = {}^1/_2$ appears in the synthetic analogs involving $[Fe_4S_4(SR)_4]^{3-}$ anions as the other part of a physical mixture with a spin $S = {}^3/_2$, and this is in particular systematically the case when the synthetic analogs are trapped in frozen

Table 4. Principal Values and Principal Directions $\mathbf{V_1}$, $\mathbf{V_2}$, and $\mathbf{V_3}$ of the *g*-Tensor for One EPR Site, and the Quasi-Orthogonal Axis Sets of Normals $\mathbf{N_1}$, $\mathbf{N_2}$, and $\mathbf{N_3}$ to Opposite Faces for the Four Cubane Sites[a]

		direction cosines with respect to				
g values		**a**	**b**	**c**	angle (deg)	with
2.027	$\mathbf{V_1}$	0.838	0	0.546		
1.930	$\mathbf{V_2}$	0	1	0		
1.904	$\mathbf{V_3}$	−0.546	0	0.838		
$\mathbf{N_1} = \mp \overrightarrow{Fe(1)Fe(4)} \times \overrightarrow{Fe(2)Fe(3)}$		0.813	±0.171	0.557	10	$\mathbf{V_1}$
$\mathbf{N_2} = - \overrightarrow{Fe(1)Fe(2)} \times \overrightarrow{Fe(3)Fe(4)}$		∓0.133	0.985	∓0.113	10	$\mathbf{V_2}$
$\mathbf{N_3} = \pm \overrightarrow{Fe(1)Fe(3)} \times \overrightarrow{Fe(2)Fe(4)}$		−0.574	±0.022	0.819	2	$\mathbf{V_3}$
$\mathbf{N_1} = \overrightarrow{\mp Fe(1)Fe(3)} \times \overrightarrow{Fe(2)Fe(4)}$		0.574	±0.022	0.819	22	$\mathbf{V_1}$
$\mathbf{N_2} = \overrightarrow{+Fe(1)Fe(2)} \times \overrightarrow{Fe(3)Fe(4)}$		±0.133	0.985	∓0.113	10	$\mathbf{V_2}$
$\mathbf{N_3} = \overrightarrow{\pm Fe(1)Fe(4)} \times \overrightarrow{Fe(2)Fe(3)}$		−0.813	±0.171	0.557	24.5	$\mathbf{V_3}$

[a] The directions are given by their direction cosines in the axis system **abc**. Two sets of normals $\mathbf{N_1}$, $\mathbf{N_2}$, and $\mathbf{N_3}$ related by the 2-fold Laue symmetry around **b** are distinguishable by the opposite signs of the four small values of direction cosines. The angle of each normal with the neighboring principal direction $\mathbf{V_1}$, $\mathbf{V_2}$, or $\mathbf{V_3}$ is specified.

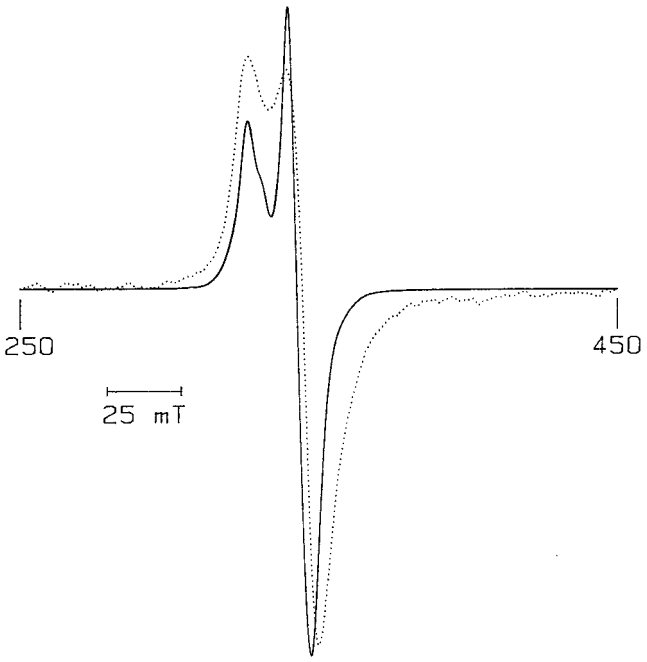

Figure 7. Comparison of the $S = 1/2$ signals in the first derivative of the X-band EPR absorption for the powder of $(Et_4N)_3[Fe_4S_4(SCH_2Ph)_4]\cdot$DMF (solid curve) and the frozen DMF 20 mM solution of $(Et_4N)_3[Fe_4S_4(SCH_2Ph)_4]$ (dotted curve). Microwave frequency is 9.23 GHz. Modulation amplitude is 0.5 mT, microwave power is 0.02 mW, and temperature is about 7 K. Frozen solution/powder gain ratio is 400.

solutions.[3a] There is a priori no reason, no symmetry factor, for the medium of frozen solutions to confer axial properties more than in the single crystals, but we note that the EPR frozen solution spectra have all exhibited axial features for the $S = 1/2$ spins.[3a] Indeed, for the frozen solution of the compound $(Et_4N)_3[Fe_4S_4(SCH_2Ph)_4]$ in DMF, the spectrum of the $S = 1/2$ part of the $[Fe_4S_4(SCH_2Ph)_4]^{3-}$ clusters presents analogy with the "axial" powder spectrum (see Figure 7 where both signals are compared). The spectrum of the $S = 1/2$ part for the frozen DMF solution is associated with apparent *g* values very close to those of the powder spectrum: 2.03 for the higher value and 1.93 for the value at zero crossing of the intense feature from Table X of ref 10 (1.92 for the latter value from our Figure 7). We can suppose that the spin $S = 1/2$ of $[Fe_4S_4(SCH_2Ph)_4]^{3-}$ in solution in DMF has in reality rhombic *g* values as in the crystal and more generally that the other spins $S = 1/2$ of the clusters $[Fe_4S_4(SR)_4]^{3-}$ in frozen solution also have rhombic *g*-tensors in spite of apparent axial features.

***g*-Strain and Spin Variety in Frozen Solution.** The signal features for the $S = 1/2$ spin of the cluster $[Fe_4S_4(SCH_2Ph)_4]^{3-}$ are broader in the frozen solution spectrum than in the powder spectrum as shown in Figure 7, despite the broadening by spin−spin interaction of the individual lines of the powder spectrum; thus, any rhombicity of the signal had even more reason to be masked in frozen solution. It is interesting to note that an apparent loss of resolution in frozen solution is also observed for the corresponding $S = 3/2$ spin of the cluster $[Fe_4S_4(SCH_2Ph)_4]^{3-}$: the signal observed in the $g = 5$ region by Carney et al. is broad and ill-resolved, like moreover all the other $g = 5$ signals of clusters of type $[Fe_4S_4(SR)_4]^{3-}$ in frozen solution, whereas the powder signal of the nonsolvated cluster $[Fe_4S_4(SCH_2Ph)_4]^{3-}$ in the $g = 5$ region is very well resolved[3a] (the powder signal can be seen in our Figure 3B). In the frozen solutions of proteins, the *g*-strain, i.e., the distribution of the real *g* values of a $S = 1/2$ spin or of the effective *g* values of a Kramers doublet of a spin $S > 1/2$, is a usual phenomenon that results from the diversity of the surroundings experienced by the paramagnetic center and leads to broadening of the signal.[17] The effects of the multiplicity of the local environments on the clusters $[Fe_4S_4(SR)_4]^{3-}$ in frozen solution must also be found in synthetic analogs. The loss of resolution observed for the signals of the spins $S = 1/2$ and $S = 3/2$ of the synthetic cluster $[Fe_4S_4(SCH_2Ph)_4]^{3-}$ in frozen solution as compared to a powder has to be a sign of the *g*-strain phenomenon in frozen solution.

But if we carry the analysis to its conclusion, the mixture of spins itself would also have to result from the variety of the local environments in frozen solution. In fact, for the cluster $[Fe_4S_4(SCH_2Ph)_4]^{3-}$ of $(Et_4N)_3[Fe_4S_4(SCH_2Ph)_4]$, the two spins $S = 1/2$ and $S = 3/2$ both coexist in frozen solution without being thermally connected whereas only one or the other of these two spins exists when the local environment is unique, i.e., in their respective single-crystal configurations. Because of the variations of the local environment, it is natural to postulate distributions of parameters that act on the relative energies of the low-lying spin states like, for instance, Heisenberg exchange (*J*) or double exchange (*B*). Then the coexistence of the two spins $S = 1/2$ and $S = 3/2$ might be explained by a distribution of such parameters in two ranges; we note that other "discrete" distributions of the effective *g* factor that preserve the spin value have already been introduced to explain the observation of multiple rhombicities, for instance, in spectra of $S = 5/2$ dilute Fe^{3+} and Mn^{2+} in silicate glass[18] and spectra of $S = 5/2$ hemoproteins or $S = 9/2$ iron−sulfur proteins in frozen solution.[15]

(17) Hagen, W. R. In *Advanced EPR Applications in Biology and Biochemistry*; Hoff, A. J., Ed.; Elsevier: Amsterdam, 1989; p 785.
(18) Griscom, D. L. *J. Non-Cryst. Solids* **1980**, *40*, 211.

And, moreover, the mixture of spin states in frozen solution for the cluster $[Fe_4S_4(SCH_2Ph)_4]^{3-}$ is quite normal since the change of the spin state of this cluster with the modification of the single-crystal structure proves the sensitivity of the spin to the environment.

The above properties—the loss of signal resolution and the mixture of spins—appear systematically for the clusters $[Fe_4S_4(SR)_4]^{3-}$ of synthetic analogs trapped in frozen solution and would have to be systematically explained by the strains provoked by the multiplicity of the local environments.

Principal *g* Directions in Cubane Geometry. Given the four, zero direction-cosines due to the alignment of $\mathbf{V_2}$ parallel to **b**, the EPR site of Table 4 has to be attributed to two crystallographic sites related by the 2-fold symmetry around **b** apart from translation. There is no symmetry reason why $\mathbf{V_2}$ should coincide exactly with **b**. Neighboring angular variations in a plane can appear to be fused if the EPR lines are broad, and thus a nondiagonal element like $(g^2)_{bc}$ is zero only within a certain tolerance. But, we have seen that the presence of the intense line in the planes $a'b'$ and ba'' proves that the EPR sites coincide and consequently that $(g^2)_{bc}$ is zero. We are aware of the very accidental nature of such a situation because even a small $(g^2)_{bc}$ would have a strong influence on the orientation of the principal directions $\mathbf{V_2}$ and $\mathbf{V_3}$ associated with *g* values particularly close to each other (1.930 and 1.904).

To insert the orthogonal set of principal directions $\mathbf{V_1}$, $\mathbf{V_2}$, and $\mathbf{V_3}$ corresponding to the EPR site of Table 4 in the geometry of a cubane site, we compare these directions with a particular axis set, the quasi-orthogonal axis set made up of the three normals to opposite faces of the cubane $\mathbf{N_1}$, $\mathbf{N_2}$, and $\mathbf{N_3}$ labeled by the number *i* of the nearest direction $\mathbf{V}_i$. For each of the two pairs of crystallographic sites related by 2-fold Laue symmetry around **b**, Table 4 gives the normals $\mathbf{N_1}$, $\mathbf{N_2}$, and $\mathbf{N_3}$ by their direction cosines in the system of axes **abc** and their angle with the corresponding direction $\mathbf{V}_i$. In the case of attribution to the first pair of sites (solution A), one of which is the cubane site whose geometry is given in the Supporting Information, the directions $\mathbf{V_1}$, $\mathbf{V_2}$, and $\mathbf{V_3}$ are found to make angles of only 10, 10, and 2° with the normals $\mathbf{N_1}$, $\mathbf{N_2}$, and $\mathbf{N_3}$, respectively. The axis set $\mathbf{V_1}$, $\mathbf{V_2}$, and $\mathbf{V_3}$ is intermediate between the axis sets $\mathbf{N_1}$, $\mathbf{N_2}$, and $\mathbf{N_3}$ of the two symmetry-related cubanes. More precisely, the direction $\mathbf{V_3}$ and the two directions $\mathbf{N_3}$ differ very little and each of the two other directions $\mathbf{V}_i$ ($i = 1, 2$) practically bisect the respective angle ($\mathbf{N}_i$, $\mathbf{N}_i'$). On the other hand, if we compare with the other pair of sites (solution B), the directions $\mathbf{V_1}$, $\mathbf{V_2}$, and $\mathbf{V_3}$ are further from the normals $\mathbf{N_1}$, $\mathbf{N_2}$, and $\mathbf{N_3}$, making angles of 22, 10 and 24.5°, respectively, with a less special geometrical arrangement of the axis set $\mathbf{V_1}$, $\mathbf{V_2}$, and $\mathbf{V_3}$ as compared with the axis sets $\mathbf{N_1}$, $\mathbf{N_2}$, and $\mathbf{N_3}$ of the two cubanes. We cannot choose among these two possible connections between the *g*-tensor and the cubanes, but it is interesting to compare them with the results obtained after γ-irradiation of the diamagnetic $[Fe_4S_4]^{2+}$ oxidation level.

In single crystals involving the diamagnetic synthetic anions $[Fe_4S_4(SR)_4]^{2-}$ we had found, after γ-irradiation, several types of spin $S = {}^1/_2$ associated with reduced $[Fe_4S_4]^+$ or oxidized $[Fe_4S_4]^{3+}$ cubanes, depending on whether the cluster $[Fe_4S_4(SR)_4]^{2-}$ had trapped or lost one electron.[2] The spin $S = {}^1/_2$ of the reduced cubane found in the γ-irradiated single crystals of the synthetic compound $(Bu_4N)_2[Fe_4S_4(SPh)_4]$ had *g* values of 2.090, 1.968, and 1.877 and thus a larger $g_{av} = 1.980$.[2b] The principal direction of maximum *g* value (2.090) was almost parallel to a cubane normal, and there were two possibilities for the other two principal directions, either (a) almost parallel to the two other normals or (b) almost parallel to a pair of Fe−Fe directions, the bisectors between the normals. Two other spins $S = {}^1/_2$ of reduced cubanes characterized also by a large g_{av}, the one named II_R found in the γ-irradiated single crystals of the synthetic compound $(Et_4N)_2[Fe_4S_4(SCH_2Ph)_4]$ ($g_{av} = 1.993$, *g* values of 2.087, 1.971, and 1.917)[2c] and the one found in $(Et_4N)_2[Fe_4S_4(S\text{-}t\text{-}Bu)_4]$ ($g_{av} = 1.987$, unpublished results) also have the principal direction of maximum *g* value near a cubane normal, but for the two other directions only a situation intermediate between (a) and (b). In the present work, the solution A with the three principal directions within 10° of the normals is close to case (a). But the solution B with the principal direction of maximum *g* value over 20° away from a normal cannot be rejected for all that, since a similar situation was found for the second type of $[Fe_4S_4]^+$ spin $S = {}^1/_2$ created in $(Et_4N)_2[Fe_4S_4(SCH_2Ph)_4]$ and named I_R.[2c] Moreover, with *g* values of 2.043, 1.948, and 1.871 and $g_{av} = 1.955$,[2c] this spin I_R has similarities with the present spin $S = {}^1/_2$.[19]

Resonance Delocalization. Electron delocalization by resonance is considered to occur in mixed-valence systems.[20] It has been introduced in addition to the Heisenberg exchange couplings for the 4Fe−4S cubanes where ions Fe^{2+} and Fe^{3+} formally coexist.[21] A resonance energy term $\pm B(S_{ij} + {}^1/_2)$ will act fully only between energetically equivalent iron sites *i* and *j*, an equivalence that would generally have to result from symmetry. When this is the case, a mixed-valence localized pair $Fe^{2+}-Fe^{3+}$ is replaced by a mixed-valence delocalized pair $Fe^{2.5+}-Fe^{2.5+}$, which is associated with a σ-bonding orbital directed across one face diagonal of the cubane.[21c] The cubane is completed by a second pair, either ferrous $Fe^{2+}-Fe^{2+}$ or ferric $Fe^{3+}-Fe^{3+}$, depending on whether it is reduced $[Fe_4S_4]^+$ or oxidized $[Fe_4S_4]^{3+}$. In the case of $[Fe_4S_4]^+$ and $[Fe_4S_4]^{3+}$ created in γ-irradiated single crystals of $[Fe_4S_4]^{2+}$ synthetic compounds, we interpreted the fact that the principal direction of maximum *g* value was close to a normal to opposite faces as the mark of some binary symmetry character,[2b,c] and we supposed that the mixed-valence pair orthogonal to this normal involved delocalization so that some equivalence of the irons was realized.[22] In the present case, the solution A, with $\mathbf{V_1}$ deviating by only 10° from a normal, is in agreement with these considerations: the normal would then be $\overrightarrow{Fe(1)Fe(4)} \times \overrightarrow{Fe(2)Fe(3)}$ and the mixed-valence delocalized pair would be Fe(1)Fe(4) or Fe(2)Fe(3). By contrast, the solution B, where the normal would be $\overrightarrow{Fe(1)Fe(3)} \times \overrightarrow{Fe(2)Fe(4)}$ and the pair would be Fe(1)Fe(3) or Fe(2)Fe(4), with $\mathbf{V_1}$ deviating by 22° from this normal, does not really lie within these expectations. We recall that, envisaging above a D_{2d} idealized symmetry for the $Fe_4S^*_4$ cubane with the $\bar{4}$ axis in the $\overrightarrow{Fe(1)Fe(2)} \times \overrightarrow{Fe(3)Fe(4)}$ direction, we retained only a 2-fold idealized axis

(19) Other spins $S = {}^1/_2$ of $[Fe_4S_4]^+$ cubanes have been found very recently in γ-irradiated single crystals of the synthetic compound $(Et_4N)_2[Fe_4S_4(SC_6H_4\text{-}o\text{-}OH)_4]$ (Le Pape, L. Doctoral Thesis, Université Joseph Fourier, Grenoble, 1994). But the singular dissymetry of the geometry of the diamagnetic $[Fe_4S_4]^{2+}$ core about one of the irons makes this case special and in particular induces a larger range of *g*-tensors for the spins $S = {}^1/_2$ of the $[Fe_4S_4]^+$ clusters.

(20) Anderson, P. W. In *Magnetism*; Rado, G. T., Suhl, H., Eds.; Academic Press: New York, 1963; Vol. 1, p 25.

(21) (a) Noodleman, L. *Inorg. Chem.* **1988**, *27*, 3677. (b) Münck, E.; Papaefthymiou, V.; Surerus, K. K.; Girerd, J.-J. In *Metal Clusters in Proteins*; Que, L., Jr., Ed.; ACS Symposium Series 372; American Chemical Society: Washington, DC, 1988. (c) Noodleman, L. *Inorg. Chem.* **1991**, *30*, 246. (d) Belinskii, M. *Chem. Phys.* **1993**, *173*, 27.

(22) On the other hand, in the study of the magnetic interactions between the nickel center and one reduced $[Fe_4S_4]^+$ cluster in the active form of the metalloenzyme Ni−Fe hydrogenase of *Desulfovibrio gigas*, good simulations of the experimental multi-frequency EPR spectra are achieved only when it is the principal direction of intermediate *g* value that is taken to be nearly perpendicular to both the mixed-valence pair and the ferrous pair (Bertrand, P.; Camensuli, P.; More, C.; Guigliarelli, B. *J. Am. Chem. Soc.* **1996**, *118*, 1426).

in the $\overrightarrow{Fe(1)Fe(4)} \times \overrightarrow{Fe(2)Fe(3)}$ direction for the $S_4Fe_4S^*_4$ cluster. Solution B does not fit since the corresponding normal is not involved. On the other hand, solution A is in full agreement since the corresponding normal is found to be the idealized 2-fold axis.

To explain the presence of a ground spin state $S = {}^3/_2$ rather than $S = {}^1/_2$ in reduced $[Fe_4S_4]^+$ cubanes, Noodleman et al. have introduced a second resonance that will produce electron delocalization between the ferrous pair $Fe^{2+}-Fe^{2+}$ and the mixed-valence localized pair $Fe^{2+}-Fe^{3+}$ and that is associated with the energy term $\pm B'(S + {}^1/_2)$.[21c,23] Such a resonance can appear in the case of a cubane of high symmetry D_{2d} because the highest occupied molecular orbital associated with the ferrous pair is a Fe−Fe δ*-antibonding orbital, whereas an orbital like the excited σ*-antibonding orbital would have no effect: consequently, the orbital mixing by symmetry lowering will weaken the coupling parameter B'.[23] Moreover, as in the case of the first resonance above, the term $\pm B'(S + {}^1/_2)$ will act fully only between energetically equivalent sites. Thus, idealized high symmetry will be doubly required to get a ground spin state $S = {}^3/_2$.[24] The geometries of the solvated and nonsolvated compounds can be compared to check an eventual symmetry gain when we skip from the spin $S = {}^1/_2$ to the spin $S = {}^3/_2$. For the $S_4Fe_4S^*_4$ core itself, the differences between the $S = {}^1/_2$ and the $S = {}^3/_2$ geometries are not significant. However, the important modifications that we have observed in the environment of the $S_4Fe_4S^*_4$ cluster from one compound to the other are in keeping with such an evolution. We have found a disordered conformation of the terminal ligands and a rather irregular location of the nearest cations in the solvated compound, whereas in the nonsolvated compound the terminal ligands extend "parallel" to the normal to opposite faces of the cubane $\overrightarrow{Fe(1)Fe(3)} \times \overrightarrow{Fe(2)Fe(4)}$, the idealized 2-fold axis, and the four nearest cations are aligned with the four other faces. In the case of the spin $S = {}^3/_2$ of the nonsolvated compound, the effective *g*-tensors of the two Kramers doublets were associated with a nonaxial zero field splitting tensor (rhombicity $\lambda \cong {}^1/_3$) and thus did not conform to an idealized high symmetry. Because the tensors might be particularly sensitive to a small symmetry lowering perturbation, the existence of the related resonance could not be excluded for all that. However, we arrive at a somewhat paradoxical situation where the spin $S = {}^3/_2$, the one supposed to be derived from high symmetry, has a maximum rhombicity and principal directions of the effective *g*-tensors all very far (more than 40°) away from the structural idealized symmetry axis whereas the spin $S = {}^1/_2$ has a real *g*-tensor relatively near axiality and a principal direction of maximum *g* value close to the structural idealized symmetry axis (solution A).

(23) Noodleman, L.; Case, D. A. In *Advances in Inorganic Chemistry*; Sykes, A. G., Ed.; Academic Press: New York, 1992; Vol. 38, p 423.

(24) As suggested by a referee for reduced $[Fe_4S_4]^+$ clusters in the case of proteins, the low symmetry environment provided by the protein could be responsible for the fact that essentially $S = {}^1/_2$ ground states are observed experimentally.

Conclusion

The crystal structure of the solvated synthetic compound $(Et_4N)_3[Fe_4S_4(SCH_2Ph)_4]\cdot DMF$ has been given. The environment of the Fe_4S_8 unit is strongly modified as compared with the case of the nonsolvated compound, and the conformation of the four terminal ligand branches CH_2Ph, well-ordered in the nonsolvated compound, becomes disordered in the solvated compound. Differences in the geometry of the paramagnetic Fe_4S_8 units must explain the different spin states observed in the two EPR studies, $S = {}^1/_2$ and $S = {}^3/_2$, but systematic differences have not been found.

Powder EPR studies have shown the progressive desolvation of the solvated compound in the glovebox, with its solid state transformation to the nonsolvated compound, and the disappearance of spin couplings in air with appearance of the EPR signature of the high spins $S = {}^5/_2$ of the irons Fe^{3+}. Differences between the powder and frozen solution EPR spectra would have as origin the *g*-strain present in frozen solution, which must imply not only a distribution of *g* for one spin value but also multiple spin values, $S = {}^1/_2$ and $S = {}^3/_2$.

The g-tensor of the solvated compound has been obtained from the single-crystal EPR study and its principal directions were found to be near the three normals to opposite faces of the Fe_4S_4 cubane. Resonance models for the spin couplings lead to more symmetric structures for $S = {}^3/_2$ spins as compared to $S = {}^1/_2$ spins, one result which is not reflected by the *g*-tensor data. Following these first two single-crystal EPR studies of spins $S = {}^1/_2$ and $S = {}^3/_2$ in the synthetic compounds $(R'_4N)_3[Fe_4S_4(SR)_4]$, studies of other compounds in the family will be undertaken to broaden our view on these questions.

Acknowledgment. We are grateful to Dr. Ronald Cox for helpful comments and to Dr. Alain Hervé for informing us about documentation on glasses. We thank Mr. Gérard Desfonds and Mr. Joël Moulin for technical assistance.

Supporting Information Available: A list of crystal data and experimental parameters (Table S1), positional parameters for the anion (Table S2) and for the cations and the solvate molecule (Table S3), anisotropic thermal parameters for the anion (Table S4), and figure of the anion (5 pages). See any current masthead page for ordering information and Internet access instructions.

JA961396A